CHAPTER 3

PRINCIPAL INSTRUMENTAL TECHNIQUES USED

3.1. Particle size analysis by FDPA

3.1.1. Theory

Particle size distribution in fly ash (Goodwin and Mitchner, 1989) and powders produced by grinding processes (Washington, 1992) fit a log-normal distribution. The log-normal distribution is given by (Allen, 1974):

$$y = [1/(\sigma_z \sqrt{2\pi})] \exp [-(z-\bar{z})^2/2\sigma_z^2] \quad (3.1)$$

where $y = d\Phi/dz$, Φ is the number, surface or weight distribution, $z = \ln D$, D represents the individual particle sizes, σ_z is the standard deviation of z, and $\bar{z}$ is the mean of the distribution (from which the mean particle size $\overline{D}$ can be calculated).

When a particle scatters light, the measured scattered light intensity may be related to the particle size; several theories are used to describe this relationship. These include the Lorentz-Mie theory (van de Hulst, 1957), the Generalised Lorentz-Mie

theory (Gouesbet et al., 1991), Geometric optics (Borhen and Huffman, 1983) and Fraunhofer diffraction.

Fraunhofer diffraction theory represents the large particle limit of the Lorentz-Mie theory for scattered light in the near forward direction. For visible incident laser light (e.g. $\lambda = 0.6328$ μm) in the near forward direction (scattering angles $\theta<11^{\circ}$) the particle size distribution may be related to the particle diameter in the 1-200 μm size range ($D>10\ \lambda/\pi$) (Bayvel and Jones, 1981). Under these conditions, diffraction (termed *Fraunhofer* diffraction) predominates over reflection and refraction, and the particle size distribution is independent of the optical properties of the sample (e.g. refractive index). The instrumental technique of Fraunhofer Diffraction Pattern Analysis (FDPA) was first introduced by Swithenbank et al. in 1977.

For a sample consisting of an ensemble of particles suspended (polydispersed) in a liquid or gas, the composite diffraction pattern produced is described mathematically by (Hirleman et al., 1984):

$$I(\theta) = I_{inc} \int_0^{\infty} (\pi^2 D^4/16\lambda^2) [2J_1(\chi)/(\chi)]^2 n(D)\, d(D) \qquad (3.2)$$

where $I(\theta)$ is the scattered intensity at the angle θ measured from the laser beam, I_{inc} is the intensity of the incident beam, $n(D)$ is the particle size (number) distribution, and $n(D)\ d(D)$ is the number of particles with sizes between D and $D+dD$.

In the Malvern instrument for FDPA the detector consists of a series of concentric rings. The energy within any detector element of inner radius s_1 and outer radius s_2 is given by (Annapragada and Adjei, 1996):

$$E(s_1, s_2) = \int_0^\infty A(D)[(J_0^2 + J_1^2)\,|\,s_1 - (J_0^2 + J_1^2)\,|\,s_2]\ d(D) \qquad (3.3)$$

where $J_n\,|\,s_i = J_n\ (\pi D s_i/\lambda)$ is the Bessel function of the n th order and first kind with argument $\pi D s_i/\lambda$, and $A(D)$ is the area fraction distribution of the particles in the sample.

Each of the detector elements exhibits a measurable response (usually a voltage) that is directly proportional to the incident energy:

$$V(s_1, s_2) = c'(s_1, s_2)\ E(s_1, s_2) \qquad (3.4)$$

where $c'(s_1, s_2)$ is a proportionality constant that can be obtained by calibrating the instrument. To obtain the actual particle size distribution the instrument must

incorporate some method (usually a software algorithm for numerical minimization) to invert the relationship between the scattered intensity pattern and the size distribution. Bayvel and Jones (1981) and Knight et al. (1991) have described their formulation of such methods.

3.1.2. Optical set-up

FDPA instrumentation, such as the Malvern Mastersizer used for this study, is based on a combination of optical analog and digital microprocessor computation. Figure 3.1 (a) shows the general optical set-up of a laser diffraction-based sizing system, and the diffraction set-up is shown in greater detail in Figure 3.1 (b).

The sample is dispersed in a suitable liquid or gas medium. In the Malvern instrument the light source comprises a 1 mW He-Ne laser (Allen, 1974). The laser is passed through the sample and the diffraction pattern produced is refracted by a Fourier transform lens and then focused onto a multi-element detector. The angle of incidence of scattered light on a Fourier lens corresponds to a particular annular position in the focal plane of the lens, regardless of the actual position of the scattering particle.

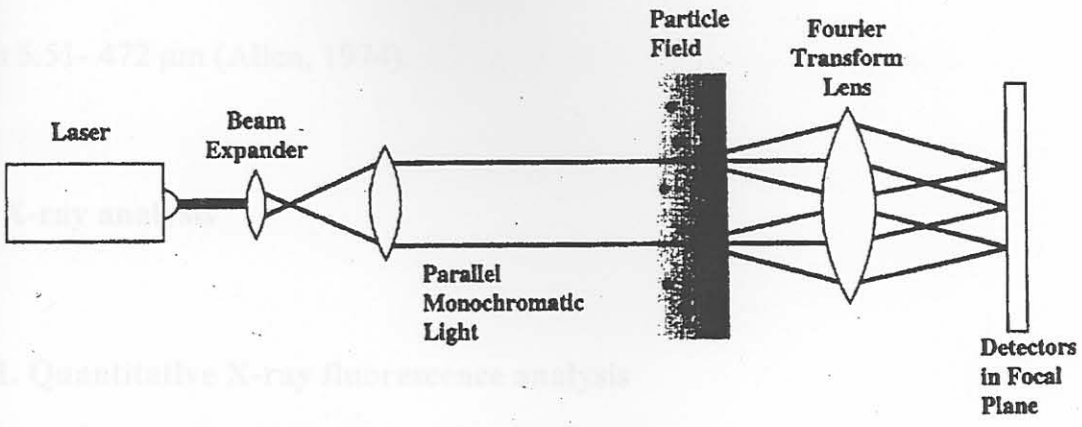

Figure 3.1 (a). Optical set-up for FDPA (Black et al., 1996).

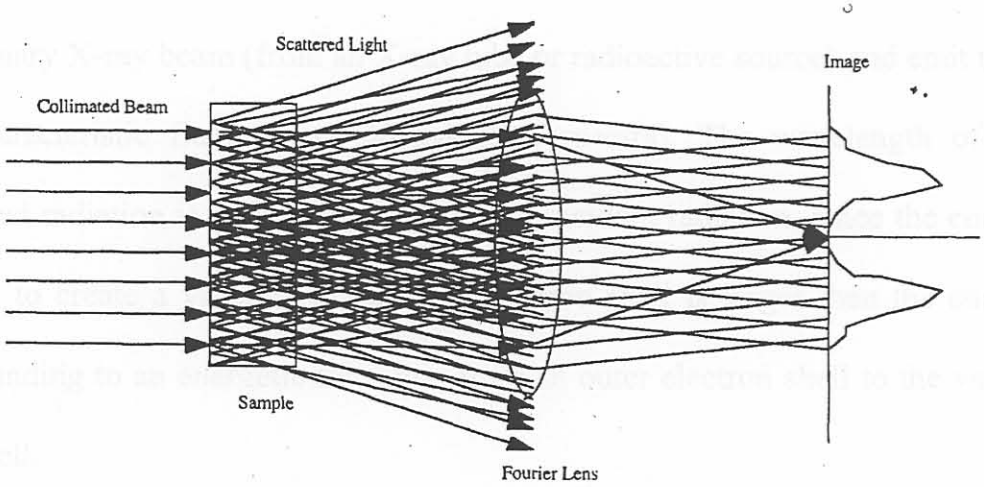

Figure 3.1 (b). Typical Fraunhofer diffraction set-up (Annapragada and Adjei, 1996).

The position of the maximum in the diffraction pattern for a given particle is determined by size so that the light intensities at different radii from the optical axis are size-dependent. The photodiode array detector in a Malvern instrument consists of a series of 31 semi-circular concentric annular detectors positioned at

the maxima of certain diffraction patterns, typically rings with diameters ranging from 5.51- 472 μm (Allen, 1974).

3.2. X-ray analysis

3.2.1. Quantitative X-ray fluorescence analysis

3.2.1.1. Theory

In X-ray fluorescence (XRF) the elements in the sample are excited by absorption of a primary X-ray beam (from an X-ray tube or radioactive source) and emit their own characteristic fluorescence X-rays (line spectra). The wavelength of the fluoresced radiation is greater than that of the incident radiation, since the energy required to create a vacancy in an inner electron shell is larger than the energy corresponding to an energetic transition from an outer electron shell to the vacant inner shell.

The intensity of the fluorescent radiation is directly proportional to the concentration of the fluorescing substance in the sample, and is also influenced by the amount of incident radiation absorbed by the sample as well as the portion of the fluorescent radiation which can be self-absorbed by the sample.

Typically, the incident radiation only penetrates a small distance relative to the thickness of the sample. The intensity I of the fluoresced radiation is given (Campbell, 1978) by:

$$I = kW/(\mu_i + \mu_f) \tag{3.5}$$

where k is a proportionality constant, W is the weight fraction of the analysed element, and μ_i and μ_f are the averaged linear absorptive coefficients for the *whole* sample at the wavelength of the incident and fluorescent radiation, respectively. I is independent of the distance penetrated into the sample since all of the incident radiation is absorbed.

If a sample x and a standard s are analysed under the same conditions, then the concentration of analyte in the sample can be calculated from:

$$C_x = C_s\,(I_x/I_s) \tag{3.6}$$

It is important to note that equation 3.10 is only useful if the sample and standard have similar composition. Generally, significant errors can occur in quantitative XRF analysis unless steps are taken to correct for matrix effects.

3.2.1.2. Instrumentation

There are two main types of XRF spectrometers in use, namely, wavelength-dispersive instruments, which use crystals to disperse the component wavelengths of the fluorescent radiation, and energy-dispersive instruments, which use electronic gates in the output circuit of the detector to discriminate between incident radiation of different wavelengths.

A block diagram of a wavelength-dispersive instrument is shown in Figure 3.2.

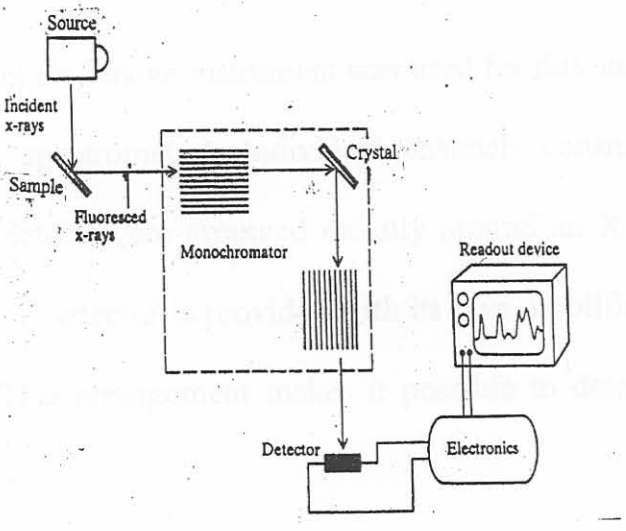

Figure 3.2. Diagram of a wavelength-dispersive XRF spectrometer (Braun, 1987).

The source is usually an X-ray tube, with a Cr or W target for long and short wavelength analysis, respectively. The sample can be solid, liquid or gas. The crystal is used to render the fluoresced radiation monochromatic by Bragg

reflection (see Section 3.2.4.1.) prior to being measured with the detector. The instrument is equipped with a detector that converts radiant energy into an electrical signal. Three types of detectors are commonly used: gas-filled detectors, scintillation counters, and semiconductor detectors (Campbell, 1978).

The detector is usually operated as a photon counter in which the individual pulse of electricity produced by a quantum of radiation is counted, and the power of the beam is recorded digitally as number of counts per unit time. The electronics amplify the pulses and select a narrow range of pulse heights for display.

A multi-channel dispersive instrument was used for this study (Figure 3.2 shows a single-channel spectrometer). Individual channels consisting of an appropriate crystal and a detector are arranged radially around an X-ray source and sample holder, and each detector is provided with its own amplifier, pulse-height selector and counter. This arrangement makes it possible to determine several elements simultaneously.

3.2.2. Qualitative X-ray diffraction analysis

3.2.2.1. Theory: Bragg's law

Bragg's law in 3-dimensional reciprocal space is given (for first-order reflections, n = 1) by (Stout and Jensen, 1989):

$$\sin\theta = \lambda/(2d_{hkl}) = \lambda/[2(h^2a^{*2} + k^2b^{*2} + l^2c^{*2} + 2hka^*b^*\cos\gamma^* + 2hla^*c^*\cos\beta^* + 2klb^*c^*\cos\alpha^*)^{1/2}] \quad (3.7)$$

where λ is the wavelength of the incident X-radiation, θ is the scattering angle, d_{hkl} is the perpendicular distance between direct lattice planes of the set with Miller indices (hkl), a^*, b^* and c^* are the mutually perpendicular axes of the reciprocal lattice, and α^*, β^* and γ^* are the angles between the axes of the reciprocal lattice.

It is evident from Bragg's law that, in principle, the interplanar spacing (and hence the identity of the crystal structure) can be determined from the measured diffraction angle if the wavelength of the incident X-ray radiation is known. The basis of qualitative XRD analysis is that an X-ray diffraction pattern is unique for each crystalline substance. Therefore, chemical identity can be assumed if an exact match can be found between the pattern of an unknown and that of an authentic sample.

3.2.4.2. Instrumentation

A diagram of a modern instrument for XRD analysis, such as the one used for this study, is shown in Figure 3.3.

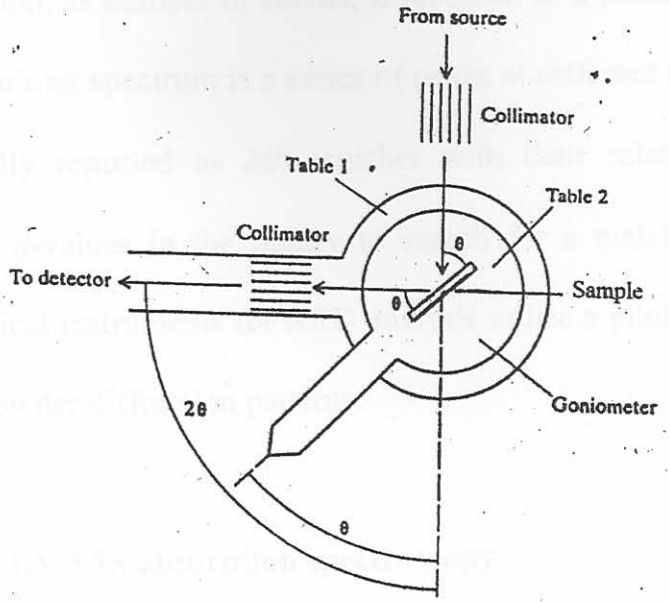

Figure 3.3. Set-up for XRD analysis (Braun, 1987).

The sample is used in the form of a fine homogeneous powder. Collimated radiation from an X-ray tube is reflected from the sample and passes through the exit collimator into the detector, which is usually a scintillation counter. The wavelength of radiation entering the detector is altered by simultaneously rotating the sample, exit collimator and detector relative to the incident radiation. A goniometer is used for this rotation. When the sample is rotated through an angle θ, the exit collimator and detector must be rotated through 2θ in order to maintain alignment. Two separate tables are used to achieve this.

Powdering the sample produces an enormous number of small crystallites oriented in every possible direction, so that a significant number will satisfy the Bragg condition for reflection from all possible interplanar spacing. The intensity of

diffracted radiation, as number of counts, is recorded as a function of the angle of rotation; the resulting spectrum is a series of peaks at different angles. These peak positions (usually reported as 2θ) together with their relative intensities are correlated with *d*-values in the library to search for a match for identification purposes. Classical instruments for XRD analysis utilise a photographic technique for recording powder diffraction patterns.

3.3. Molecular UV/VIS absorption spectroscopy

3.3.1. Theory: The Bouguer-Lambert-Beer (BLB) law

The BLB law is a statement to the effect that the absorbance A of a solution is directly proportional to the path length b through the solution and the concentration c of the absorbing species:

$$A = \varepsilon_\lambda bc \tag{3.8}$$

where ε_λ is a wavelength-dependent proportionality constant. Absorption of UV/VIS radiation (ca. 200-800 nm) generally results from excitation of bonding electrons. For the analysis of phosphate ion the most important transitions types are expected to be n→ π* and π→ π*. For quantitative analysis ε_λ is usually

evaluated from the slope of the linear calibration plot of A versus c (concentration of analyte in several laboratory standard solutions) using regression analysis.

3.3.2. Instrumentation

A schematic diagram of the optical system of the UV/VIS instrument used for this study, a Shimadzu UV-150 digital double-beam spectrophotometer, is shown in Figure 3.4 (a). The light beam is selected between the W (325–1000 nm) and D_2 (200–325 nm) lamps for the visible and ultraviolet regions respectively by the light source selecting mirror M_1, forms an image on the entrance slit S_1, and is led into the monochromator. The Czerny-Turner grating monochromator consists of S_1, M_2, G, M_3, M_4 and S_2, and a monochromatic light with 5 nm band width is taken out from the exit slit S_2. The monochromatic light is divided into the sample and reference beams by the half-mirror M_6, passes through the cell holder and strikes the silicon photocell detector.

Figure 3.4 (b) shows the electronic system of the instrument. The difference between the photo currents i_S from the sample detector and i_R from the reference detector is taken by the subtracter after individual logarithmic conversion. The output from the subtracter is multiplied by a factor k to become $-k \log (i_S/i_R)$, where k is chosen in such a way that an output voltage of 1 V corresponds to a unit

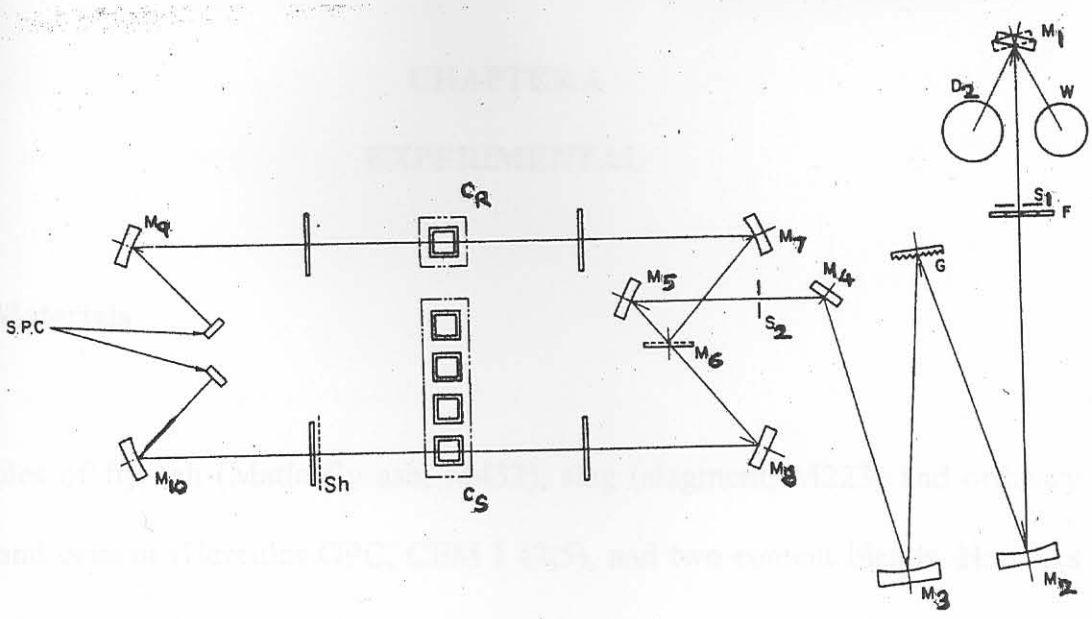

W:	Tungsten lamp	G:	Diffraction Grating
D_2:	Deuterium lamp	F:	Filters
M_1~M_{10}	Mirrors	C_R, C_S:	Reference cell, Sample cell
M_6:	Half-mirror	SPC:	Silicon photo cell
S_1, S_2:	Slit	Sh:	Shutter

Figure 3.4 (a). Schematic diagram of the Shimadzu UV-150 optical system (Shimadzu, 1994).

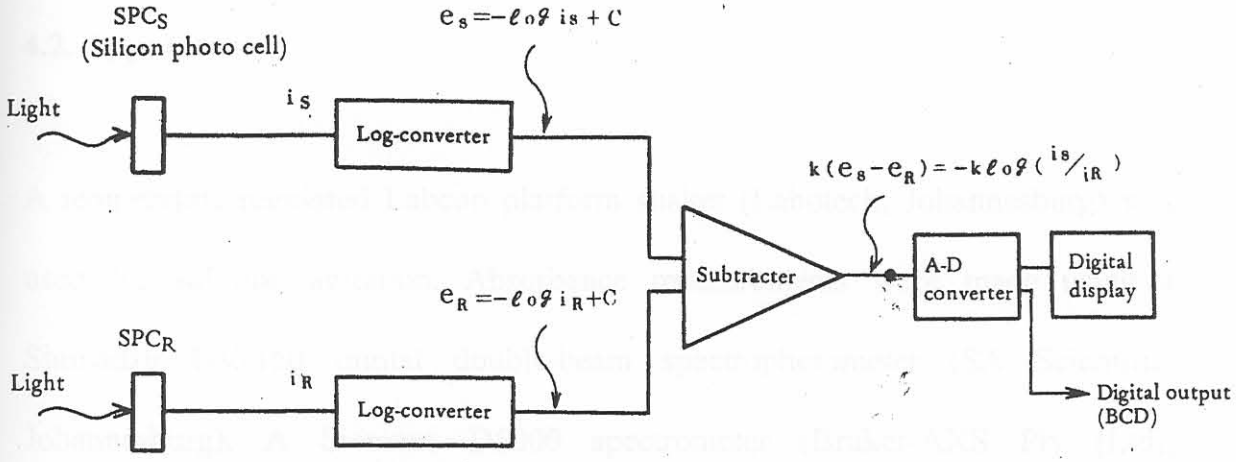

Figure 3.4 (b). Schematic of the Shimadzu UV-150 electronic system (Shimadzu, 1994).

absorbance, i.e. i_S/i_R = 1/10. The output signal is displayed on the digital meter after A-D (analogue-to-digital) conversion.